Econometric Theory, **0**, 2026, 1–28.
doi:10.1017/S0266466626100504

ESTIMATION OF RANDOM CYCLES IN PERSISTENT TIME SERIES

KARIM M. ABADIR
Imperial College London

NATALIA BAILEY
Monash University

WALTER DISTASO
ADIA, Imperial College London, UNIME

LIUDAS GIRAITIS
Queen Mary University of London

A number of economic, financial, and climatic time series exhibit persistent cycles which are characterized by time-dependence patterns and peaks in the spectrum. In this article, we introduce a class of semiparametric cyclical–memory processes which enable the modeling of random cyclical patterns in stationary and non-stationary time series. We develop a theoretical background and asymptotic estimation theory for the frequency of a cycle represented by the location of a peak in the spectrum. The estimation procedure is easy to implement and allows for the construction of narrow confidence intervals around the location point. Monte Carlo simulations confirm the good finite sample performance of our estimator. We illustrate our method with three empirical applications. We uncover (quasi-)periodic cycles in macroeconomic series, both nominal and real (U.S. nominal GDP and real industrial production), and CO_2 concentration levels.

1. INTRODUCTION

Analysis of data exhibiting persistent regular patterns is important in many empirical studies. For example, a large body of literature is dedicated to the investigation and extraction of periodic or quasi-periodic behavior in macroeconomic, geophysical, and climatic time series. In applications, it is common to make a distinction between cyclicality and seasonality. Seasonal or periodic fluctuations are viewed to be generated by factors, such as the quarter or month of the year, day of the week, etc. As such, seasonality is considered to be of a fixed and, often, of known period. On the other hand, cyclicality refers to oscillations that are determined partly by an exterior impulse which may operate irregularly. Hence, cyclicality is not of fixed period but "[. . .] takes place within such limits that it is

We thank the Editor, Co-Editor, and three Referees for constructive comments and valuable suggestions that have helped to improve the article. Address correspondence to Liudas Giraitis, Queen Mary University of London, UK, E-mail: l.giraitis@qmul.ac.uk

© The Author(s), 2026. Published by Cambridge University Press. This is an Open Access article, distributed under the terms of the Creative Commons Attribution-NonCommercial-NoDerivatives licence (https://creativecommons.org/licenses/by-nc-nd/4.0), which permits non-commercial re-use, distribution, and reproduction in any medium, provided that no alterations are made and the original article is properly cited. The written permission of Cambridge University Press or the rights holder(s) must be obtained prior to any commercial use and/or adaptation of the article.

Downloaded from https://www.cambridge.org/core. IP address: 92.41.158.104, on 12 Aug 2026 at 10:47:18, subject to the Cambridge Core terms of use, available at https://www.cambridge.org/core/terms. https://doi.org/10.1017/S0266466626100504

reasonable to speak of an average period [. . .]"—Frisch (1933). The lengths of these quasi-cycles typically exceed two years, are not known *a priori*, and are less clearly identifiable due to the additional variability of their sample ACFs.

In this article, we focus on the estimation theory for the frequency of a cycle. We make no distinction between the terms "seasonality" and "cyclicality" since they have the same spectral characterization, and consider from the outset that the length of an oscillation or cycle is unknown. Correctly establishing this quantity enables the accurate representation of the cyclical patterns characterizing the underlying data and avoids over- or under-parameterizations in model building. This, then, can provide reliable guidance for policy adjustments. Our key objective is to produce a statistical procedure for the estimation of the length of a cycle in an unrestrictive setting. For this purpose, we also introduce a class of semiparametric processes that enables modeling of cyclical behavior in stationary and non-stationary environments.

First, we provide a formal exposition of this new generic class of semiparametric *cyclical memory* CM(ω, d) processes and describe its main features. These processes can reproduce random cyclical patterns with a pole at frequency ω on $[0, \pi]$[1] and can be stationary or non-stationary as determined by the memory parameter d. They are written as

$$X_j = \mu + \cos(\omega j) Z_j + \sin(\omega j) Z'_j, \quad j \in \mathbb{Z}, \tag{1.1}$$

where $\{Z_j\}$ is an integrated I(d) process, $\{Z'_j\}$ is its independent copy, and μ is an intercept. Parameter d in the I(d) process Z_j can range between 0 and 3/2 and, hence, describes both stationary and non-stationary alternatives, while the spectral density of Z_j (pseudo-spectral density in the non-stationary case) has a peak at frequency 0. This generates a peak at frequency ω in the spectrum f_X of $\{X_j\}$ which constitutes the main feature of CM processes and defines the length of the quasi-cycle as $\lambda = 2\pi/\omega$. The sharpness of the peak is characterized by the same integration (memory) parameter $d \in (0, 3/2)$ as for Z_j and it does not vary with ω. Differencing our cyclical process X_t does *not* remove persistence when $\omega \neq 0$, even if fractional differencing were to be used, because the peak of the spectrum is not at frequency zero. This has practical implications that will be illustrated in our empirical applications. A special case of CM models arises from the macroeconomic model of Abadir and Talmain (2002) that incorporates the effects of aggregation on the persistence of economic activity variables, as explained in Abadir and Talmain (2011), hence its relevance in economics (and beyond). Independently, Proietti and Maddanu (2024) also provide a description of a parametric version of the CM process, see Section 4 below (they call it *a sinusoidal waveform process*) and discuss its properties and applications but only in the stationary case. For alternative modeling approaches of non-stationary cyclical time series, see, for example, del Barrio Castro, Rodrigues, and Taylor

[1] We follow the time series usage of "pole" to refer to singularities ω^{-p}, where p is not necessarily an integer (cf. usage in complex analysis).

Downloaded from https://www.cambridge.org/core. IP address: 92.41.158.104, on 12 Aug 2026 at 10:47:18, subject to the Cambridge Core terms of use, available at https://www.cambridge.org/core/terms. https://doi.org/10.1017/S0266466626100504

(2018, 2019); del Barrio Castro, Cubadda, and Osborn (2022), Maddanu (2022), and Kang and Marmer (2024).

Next, we set up the estimation theory for parameter ω in the CM(ω, d) model. We estimate ω by the Fourier frequency $\widehat{\omega}$ which maximizes the periodogram of cyclical time series X_j. Such an estimator is easy to compute. In finite samples, it becomes more precise as the memory parameter d increases and, crucially, does not hinge on a particular parametric specification for Z_j. We establish n^{-1} rate of consistency (n being the sample size) for the estimator $\widehat{\omega}$ as well as its asymptotic distribution. Monte Carlo simulations confirm the validity of the asymptotic theory and illustrate its properties in finite samples. They show the location of the pole ω to be confined with high probability (>95%) within confidence intervals comprising of up to two Fourier frequencies, $\widehat{\omega} \pm u_j$, $j = 1, 2$, where $u_j = 2\pi j/n$, when $d \geq 0.4$. Though the width of these confidence bands is linked to the memory parameter d, simulation experiments confirm that for d in excess of 0.35 or 0.4 the true pole ω lies within one or two Fourier frequencies around the frequency $\widehat{\omega}$ with high probability (see Section 3).

For modeling cyclical behavior in empirical work, we introduce a parametric auto-regressive cyclically-integrated moving-average ARCIMA(p, ω, d, q) model. The ARCIMA model allows parametric modeling of cyclical patterns both in stationary and non-stationary time series. It falls within the class of cyclical memory CM(ω, d) processes. This model is obtained from the CM(ω, d) specification (1.1) by setting $\{Z_j\}$ to be a parametric fractional ARIMA(p, d, q) process, with $d \in (0, 3/2)$,

$$\phi(B)(1-B)^d Z_j = \theta(B)\zeta_j, \tag{1.2}$$

where B is the backshift operator, and polynomials $\phi(B)$ and $\theta(B)$ satisfy the standard assumptions of a stationary ARMA model. The (pseudo-)spectrum of ARIMA process Z_j in (1.2) exhibits an infinite peak at zero frequency consistent with the operator $(1-B)^d$ and memory parameter d only. If $p \neq 0$ or $q \neq 0$, then the shape of the infinite peak in the spectrum of the ARIMA process Z_j at zero frequency is adjusted to reflect the relevant (bounded) spectrum of the ARMA components. The cyclical model (1.1) shifts this peak to the frequency ω in the spectrum of X_j which can be estimated using the estimation methods and results established for the CM(ω, d) model (see Section 3).

Estimation of other parameters of Z_j, including $d \in (0, 3/2)$, is challenging and beyond the scope of this article. Our empirical findings of Section 6 on CO_2 concentration suggest that, when fitting a stationary ARCIMA model with predetermined cyclical frequencies, as in Proietti and Maddanu (2024), maximum likelihood estimation can result in over-parameterization and estimates of d that hit the upper bound of the stationary region ($\hat{d} \approx 1/2$). Theoretical results of our article on estimation of ω can be extended easily to the case of multiple poles. However, testing for the existence of cyclical patterns (a pole ω in the spectrum) requires a separate theoretical analysis.

Downloaded from https://www.cambridge.org/core. IP address: 92.41.158.104, on 12 Aug 2026 at 10:47:18, subject to the Cambridge Core terms of use, available at https://www.cambridge.org/core/terms. https://doi.org/10.1017/S0266466626100504

The closest alternative to the stationary version of the above parametric ARCIMA(p,ω,d,q) model is the parametric Gegenbauer auto-regressive moving-average (GARMA) model introduced by Andel (1986) and Gray, Zhang, and Woodward (1989, 1994). This emerged from the earlier idea of Granger and Joyeux (1980) and Hosking (1981) to use a generalization of a fractionally differenced model to allow for seasonality in a time-series process. The GARMA model for seasonal time-series process $\{X_j\}$ is given by

$$\phi(B)\left(1-2\cos(\omega)\cdot B+B^2\right)^d X_j=\theta(B)\zeta_j,\quad j\in\mathbb{Z}, \tag{1.3}$$

where $0\le\omega\le\pi$, $|d|<1/2$, $\{\zeta_j\}$ is a white noise $(0,\sigma_\zeta^2)$ sequence, and $\phi(B)$ and $\theta(B)$ are as before. The GARMA model with memory parameter $0<d<1/2$ allows the modeling of long-term persistence and quasi-periodic behavior, and its correlation function resembles a superposition of hyperbolically damped sine waves. The spectral density of such time series again has a pole at ω on $[0,\pi]$.

While the ARCIMA specification falls within the class of our proposed cyclical memory CM(ω,d) processes, GARMA and CM models are not nested. Hence, the GARMA model does not share some of ARCIMA's benefits, including the ease of simulation and the uniform persistency over ω (see Section 2). For example, unlike ARCIMA, simulation of a Gaussian GARMA process using algorithm of Davies and Harte (1987) is not straightforward. This algorithm requires knowledge of the autocovariance function, which for a GARMA$(0,d,0)$ process is rather complicated, and not available for a GARMA model with multiple poles. Further, for a given d, the sharpness of peak in the spectrum of ARCIMA process is uniform over the location of the peak, ω, while for GARMA, it doubles to $2d$ at $\omega=0$ (see Section 4). Regarding estimation, focusing solely on the estimation of ω, Hidalgo and Soulier (2004) obtain a consistency rate $n^{-1+\epsilon}$ for a Gaussian GARMA model, which is lower than our consistency rate of n^{-1} for CM(ω,d) models, and do not establish the asymptotic distribution of $\widehat{\omega}$. Overall, when ω is unknown, parametric estimation of the GARMA model becomes significantly harder (see Giraitis, Hildago, and Robinson, 2001).

Our empirical illustration covers three examples from macroeconomics and climate science. We investigate the presence of persistent regular patterns (periodic and quasi-periodic) in U.S. nominal GDP over the period Q1-1956 to Q4-2019, U.S. real industrial production (IP) over the period August 1977 to December 2019, and CO_2 concentration over the period May 1978 to December 2020. In all cases, it is evident that well-defined peaks in the periodogram are indicative of persistent cyclical patterns, while less pronounced/ambiguous peaks reflect reduced evidence for cyclical structure and require further investigation using complementary tools.

The article is organized as follows. Section 2 outlines the formal definition of the semiparametric class CM(ω,d) of cyclical models, together with their auto-covariance and spectral density properties. Section 3 presents theoretical results for estimation of the location parameter ω, based on the estimator $\widehat{\omega}$ for CM(ω,d) processes. Section 4 introduces the parametric ARCIMA model. Section 5 reports Monte Carlo simulation results, while Section 6 presents empirical examples from

Downloaded from https://www.cambridge.org/core. IP address: 92.41.158.104, on 12 Aug 2026 at 10:47:18, subject to the Cambridge Core terms of use, available at https://www.cambridge.org/core/terms. https://doi.org/10.1017/S0266466626100504

macroeconomics and climate research. Proofs and additional simulation results are provided in Appendixes A–C of the Supplementary Material.

2. SEMIPARAMETRIC CYCLICAL–MEMORY MODEL

In this section, we introduce a class of semiparametric CM(ω, d) cyclical–memory processes that enable the modeling of regular cyclical patterns in stationary and non-stationary time series. These models are characterized by two parameters, ω and d, for cycle and memory, respectively. They have spectral density (pseudo-spectral density in the non-stationary case) that is unbounded at frequency $\omega \in (0, \pi)$ and the sharpness of the peak is defined by the memory parameter $d \in (0, 3/2)$. This domain of d covers most time series of practical interest. It can be extended to $d > 3/2$ in the same way that we extend the stationary I(d), $d \in (0, 1/2)$ process to $d \in (1/2, 3/2)$ in Definition 2.1 below.

The precise definition of the semiparametric CM(ω, d) model with a pole at frequency $\omega \in (0, \pi)$ in the spectrum uses a semiparametric integrated I(d) process, the spectral density of which has a pole at zero frequency, $\omega = 0$.

DEFINITION 2.1. (a) $\{Z_j\}$ *is said to be an* I(d) *process with* $|d| < 1/2$ *if:*
(i) $\{Z_j, j \in \mathbb{Z}\}$ *is a stationary linear process of the form*

$$Z_j = \sum_{k=0}^{\infty} a_k \zeta_{j-k}, \quad a_0 = 1, \quad \sum_{k=0}^{\infty} a_k^2 < \infty, \tag{2.1}$$

where $\{\zeta_j\}$ *is an i.i.d. sequence with* $\mathrm{E}\zeta_j = 0$, $\mathrm{E}\zeta_j^2 = \sigma_\zeta^2$, *and* $\mathrm{E}\zeta_j^4 < \infty$.
(ii) *The spectral density function of* $\{Z_j\}$ *can be written as*

$$\begin{aligned} f_Z(u) &= (\sigma_\zeta^2/2\pi)\Big|\sum_{k=0}^{\infty} \mathrm{e}^{\mathrm{i}ku} a_k\Big|^2, \qquad u \in \Pi = [-\pi, \pi], \\ &= |u|^{-2d} g(u), \end{aligned} \tag{2.2}$$

where $g > 0$ *is a continuous function bounded away from* 0 *and* ∞.
(iii) *The covariance function* $\gamma_Z(k) = \mathrm{cov}(Z_k, Z_0) = \int_{-\pi}^{\pi} \mathrm{e}^{\mathrm{i}ku} f_Z(u) du$ *and the coefficients in* a_k *in (2.1) satisfy*

$$\gamma_Z(k) = c_\gamma k^{-1+2d} + o(k^{-1+2d}) \quad \text{if } d \neq 0, \tag{2.3}$$

$$\sum_{j=0}^{\infty} |a_j| < \infty \text{ for } d = 0; \quad \sum_{j=0}^{\infty} a_j = 0 \text{ for } d < 0.$$

(b) *A process* $\{Z_j\}$ *is said to be an* I(d) *with* $d \in (1/2, 3/2)$ *process if* $\nabla Z_j = Z_j - Z_{j-1}$ *is an* I$(d-1)$ *process as defined in part (a). We assume that* $Z_0 = O_p(1)$. *In this case,* $d - 1 \in (-1/2, 1/2)$.

Downloaded from https://www.cambridge.org/core. IP address: 92.41.158.104, on 12 Aug 2026 at 10:47:18, subject to the Cambridge Core terms of use, available at https://www.cambridge.org/core/terms. https://doi.org/10.1017/S0266466626100504

For $0 < d < 1/2$, the process $\{Z_j\}$ is stationary with long memory, and its spectral density f_Z is unbounded at the zero frequency: $f_Z(u) \sim c|u|^{-2d}$ as $u \to 0$. For $1/2 < d \leq 1$, an analogous property holds for the pseudo-spectral density f_Z (see (2.11)).

Remark 2.1. Parametric stationary ARIMA(p,d,q) processes are I(d) processes and satisfy Assumption 3 below (see Chapters 3 and 7 and Remark 6.2.2 in Giraitis, Koul, and Surgailis, 2012). The condition $\sum_{k=0}^{\infty} a_k = 0$ for $d < 0$ is aligned with (2.2), since $2\pi f(0) = \sum_{k=-\infty}^{\infty} \gamma_Z(k) = \sigma_\zeta^2 (\sum_{k=0}^{\infty} a_k)^2 = 0$.

We can now introduce a new class of semiparametric cyclical–memory processes, denoted CM(ω,d), defined as follows.

DEFINITION 2.2. *A process $\{X_j\}, j \in \mathbb{Z}$, is said to be a* CM$(\omega,d)$ *cyclical–memory process with parameters $\omega \in (0,\pi)$ and $d \in (0,3/2)\backslash\{1/2\}$, if it can be written as*

$$X_j = \mu + \cos(\omega j) Z_j + \sin(\omega j) Z_j', \quad j \in \mathbb{Z}, \tag{2.4}$$

where $\{Z_j\}$ is an I(d) *process, $\{Z_j'\}$ is an independent copy of $\{Z_j\}$, and μ is an intercept.*

The next theorem provides the main properties of a stationary CM(ω,d) model with $0 < d < 1/2$. It shows that these processes are covariance stationary, their autocovariance functions decay as hyperbolically damped sine waves, and their spectral densities have an infinite peak at frequency ω, remaining bounded and continuous at all other frequencies on the spectrum.

We assume that f_Z in (2.2) is extended to the real line $\mathbb{R}$ with period 2π.

THEOREM 2.1. *Suppose that $0 < \omega < \pi$ and $0 < d < 1/2$. Then the* CM(ω,d) *process $\{X_j\}$ in (2.4) has the following properties:*

(i) *$\{X_j\}$ is covariance stationary, with autocovariance function γ_X and spectral density f_X given by*

$$\gamma_X(k) = \cos(\omega k)\gamma_Z(k), \qquad k \geq 0, \tag{2.5}$$

$$f_X(u) = (f_Z(u-\omega) + f_Z(u+\omega))/2 = \big||u|-\omega\big|^{-2d} g_X(u), \qquad u \in \Pi,$$

where $g_X(u)$ is a continuous even function bounded away from zero and infinity.

(ii) *Let a_k, ζ_k be as in (2.1), and let $\{\zeta_k'\}$ be an independent copy of $\{\zeta_k\}$. Then*

$$X_j = \mu + \sum_{k=0}^{\infty} a_k \xi_{j,k}, \quad \xi_{j,k} = \cos(\omega j)\zeta_{j-k} + \sin(\omega j)\zeta_{j-k}', \quad j \in \mathbb{Z}, \tag{2.6}$$

$$= \mu + \sum_{k=0}^{\infty} a_k \cos(\omega k)\eta_{j-k} + \sum_{k=0}^{\infty} a_k \sin(\omega k)\eta_{j-k}^*, \tag{2.7}$$

where

$$\eta_k := \cos(k\omega)\zeta_k + \sin(\omega k)\zeta_k', \quad \eta_k^* := -\sin(\omega k)\zeta_k + \cos(\omega k)\zeta_k'.$$

Downloaded from https://www.cambridge.org/core. IP address: 92.41.158.104, on 12 Aug 2026 at 10:47:18, subject to the Cambridge Core terms of use, available at https://www.cambridge.org/core/terms. https://doi.org/10.1017/S0266466626100504

In (2.6), for each j, $\{\xi_{j,k}, k \in \mathbb{Z}\}$ *is an i.i.d.* $(0, \sigma_\zeta^2)$ *sequence. In (2.7), the sequences* $\{\eta_k\}$ *and* $\{\eta_k^*\}$ *are mutually uncorrelated sequences of independent variables with* $\mathrm{E}\eta_k = \mathrm{E}\eta_k^* = 0$ *and* $\mathrm{E}\eta_k^2 = \mathrm{E}\eta_k^{*2} = \mathrm{E}\zeta_k^2 = \sigma_\zeta^2$.

Proof. See Appendix A of the Supplementary Material. Representation (2.7) extends Proposition 1 in Proietti and Maddanu (2024), originally established for Gaussian processes, to the case of non-Gaussian cyclical–memory processes. □

For a non-stationary cyclical process $X_j \sim \mathrm{CM}(\omega, d)$, $d \in (1/2, 3/2)$, cyclical patterns can be captured by the sample covariance function $\widehat{\gamma}_X(k)$ and the periodogram $I_X(u)$:

$$\widehat{\gamma}_X(k) := \int_{-\pi}^{\pi} \mathrm{e}^{\mathrm{i}ku} I_X(u)\mathrm{d}u \quad \text{and} \quad I_X(u) := (2\pi n)^{-1} \Big| \sum_{j=1}^{n} \mathrm{e}^{\mathrm{i}ju} X_j \Big|^2.$$

Theorem 2.2 shows that (on average) $\widehat{\gamma}_X(k)$ exhibits the same cyclical behavior as $\gamma_X(k)$ in the stationary case in (2.5).

THEOREM 2.2. *Let* $0 < \omega < \pi$ *and* $d \in (1/2, 3/2)$. *Suppose that* $X_j \sim \mathrm{CM}(\omega, d)$ *and that* $Z_j \sim \mathrm{I}(d)$ *with* $\mathrm{E}(Z_j) = 0$. *Then,*

$$\mathrm{E}[\widehat{\gamma}_X(k)] = \cos(\omega k)\mathrm{E}[\widehat{\gamma}_Z(k)], \ k \geq 0. \tag{2.8}$$

Proof. See Appendix A of the Supplementary Material. □

In the stationary case, when $d \in (0, 1/2)$, the spectral densities $f_Z(u), f_X(u)$ and their empirical counterparts (the periodograms $I_Z(u), I_X(u)$) are related as follows: as $n \to \infty$,

$$\begin{aligned} \mathrm{E}I_Z(u) &= f_Z(u) + o(1), \ u \neq 0, \qquad u \in \Pi, \\ \mathrm{E}I_X(u) &= f_X(u) + o(1), \ u \neq \omega. \end{aligned} \tag{2.9}$$

Theorem 3.1 in Section 3 shows that (2.9) remains valid for non-stationary $\mathrm{CM}(\omega, d)$ processes with $d \in (1/2, 1]$, provided that the spectral densities are replaced by pseudo-spectral densities:

$$\begin{aligned} f_Z(u) &= |1 - \mathrm{e}^{\mathrm{i}u}|^{-2}(f_{\nabla Z}(u) + f_{\nabla Z}(0)), \qquad u \in \Pi, \\ f_X(u) &= \big(f_Z(u-\omega) + f_Z(u+\omega)\big)/2, \end{aligned} \tag{2.10}$$

where $f_Z(u)$ is extended periodically to $\mathbb{R}$. These functions are not integrable. Notice that $f_{\nabla Z}(0) = 0$ for $d \in (1/2, 1)$. These pseudo-spectral densities exhibit the same pattern of cyclical behavior as for $\{Z_j\}$, $\{X_j\}$ in the stationary case:

$$f_Z(u) = |u|^{-2d} g_Z(u), \quad f_X(u) = |u-\omega|^{-2d} g_X(u), \qquad u \in \Pi, \tag{2.11}$$

where $g_Z(u)$ and $g_X(u)$ are continuous functions bounded away from zero and infinity.

Downloaded from https://www.cambridge.org/core. IP address: 92.41.158.104, on 12 Aug 2026 at 10:47:18, subject to the Cambridge Core terms of use, available at https://www.cambridge.org/core/terms. https://doi.org/10.1017/S0266466626100504

3. ESTIMATION OF ω

In this section, we discuss the estimation of the parameter ω of a cyclical process $X_j \sim \mathrm{CM}(\omega, d)$ when $0 < d < 3/2$ and $d \neq 1/2$. The estimation of ω will be based on the periodogram:

$$I_X(u) = |w_X(u)|^2, \quad w_X(u) := (2\pi n)^{-1/2} \sum_{j=1}^{n} \mathrm{e}^{-\mathrm{i}uj} X_j, \quad u \in \Pi,$$

where $w_X(u)$ is the discrete Fourier transform (DFT), both based on the sample $X_1, \ldots, X_n$.

For $d \in (0, 1/2)$, the spectral density $f_X(u)$, $u \in \Pi$, of a stationary cyclical process $\{X_j\}$ has an infinite peak at the frequencies $u = \pm\omega$. For $d \in (1/2, 1]$, the cyclical times series $\{X_j\}$ is non-stationary, and its pseudo-spectral density $f_X(u)$, defined in (2.10), also has an infinite peak at frequencies $\pm\omega$ (see Theorem 3.2). Although the periodogram $I_X(u)$ is only a mean consistent estimator of $f_X(u)$ at the continuity points $u \in \Pi \backslash \{\pm\omega\}$, one can expect that the location of the maximum of the periodogram will converge to the location of the maximum of $f_X(u)$, $0 \leq u \leq \pi$, that is, ω, at a fast rate. This is confirmed by Theorem 3.3 below.

We define the estimator $\widehat{\omega}$ of ω as the maximizer of the periodogram:

$$\widehat{\omega} := \mathrm{argmax}_{k=1,\ldots,\widetilde{n}} I_X(u_k), \tag{3.1}$$

over the set of Fourier frequencies $u_j = 2\pi j/n, j = 1, \ldots, \widetilde{n} := \lfloor n/2 \rfloor - 1$. Note that $u_{\widetilde{n}} \sim \pi$.

This estimator was introduced by Hidalgo and Soulier (2004) for the estimation of ω in a stationary Gaussian GARMA model. In their Theorem 2, they establish the consistency rate $\widehat{\omega} - \omega = O_p(n^{-1+\epsilon})$ for any $\epsilon > 0$ and abstain from deriving the asymptotic distribution. By comparison, we establish the consistency rate $O_p(n^{-1})$ in estimation of ω for both stationary and non-stationary $\mathrm{CM}(\omega, d)$ processes (see Theorem 3.2 below). Furthermore, in Theorem 3.3, we derive the asymptotic distribution for $\widehat{\omega}$.

For simplicity, in the next theorems, we assume that the pole ω is at a Fourier frequency $\omega = u_{k_0}$, where $k_0 := k(n)$ is an integer. and suppose that

$$0 < \delta \leq \omega \leq \pi - \delta, \quad n \geq 1, \quad (\text{for some } 0 < \delta < 1/2). \tag{3.2}$$

Establishing the consistency rate and asymptotic distribution for $\widehat{\omega}$ requires additional assumptions on the $\mathrm{I}(d)$ process $\{Z_j\}$ that appear in the definition (2.4) of the $\mathrm{CM}(\omega, d)$ process $\{X_j\}$.

By Definition 2.1(i), for $0 < d < 1/2$, $Z_j = \sum_{k=0}^{\infty} a_k \zeta_{j-k}$ is a stationary linear process. For $1/2 < d < 3/2$, $\nabla Z_j = \sum_{k=0}^{\infty} a'_k \zeta_{j-k}$ also can be written as a stationary linear process. We impose the following additional assumptions on their transfer functions:

$$A_Z(u) = \sum_{j=0}^{\infty} \mathrm{e}^{\mathrm{i}ju} a_j, \quad A_{\nabla Z}(u) = \sum_{j=0}^{\infty} \mathrm{e}^{\mathrm{i}ju} a'_j, \quad |u| \leq \pi. \tag{3.3}$$

Downloaded from https://www.cambridge.org/core. IP address: 92.41.158.104, on 12 Aug 2026 at 10:47:18, subject to the Cambridge Core terms of use, available at https://www.cambridge.org/core/terms. https://doi.org/10.1017/S0266466626100504

Assumption 1. I(d) process $\{Z_j\}$ in (2.4) has the following properties:
For $0 < d < 1/2$, assume that $\mathrm{E}|\zeta_j|^q < \infty$ for some $q > 1/4d$. Moreover,

$$\left|(\mathrm{d}/\mathrm{d}u)A_Z(u)\right| \le C|u|^{-1-d}, \quad \text{for } d \in (0, 1/2), \tag{3.4}$$

$$\sum_{k=0}^{\infty} |a_j'| < \infty, \quad \text{for } d = 1, \tag{3.5}$$

$$\left|(\mathrm{d}/\mathrm{d}u)A_{\nabla Z}(u)\right| \le C|u|^{-d}, \quad \text{for } d \in (1/2, 3/2),\ d \ne 1, \tag{3.6}$$

where C does not depend on $u \in \Pi$.

We consider the estimation of the parameter ω by the same estimator $\widehat{\omega}$ both when the cyclical CM(ω, d) process $\{X_j\}$ is stationary and non-stationary. The following theorem provides insights on why, for a non-stationary cyclical process, the periodogram also tends to peak around the frequency ω. It relates the periodograms I_X, I_Z to the pseudo-spectral densities f_X, f_Z given in (2.10). Recall that f_X has an infinite pole at frequency ω, while f_Z has one at frequency 0.

THEOREM 3.1. *Let $0 < \omega < \pi$ and $d \in (1/2, 1]$. Suppose that $X_j \sim \mathrm{CM}(\omega, d)$ and $Z_j \sim \mathrm{I}(d)$ satisfy Assumption 1. Then, for any $\epsilon > 0$, as $n \to \infty$,*

$$\begin{aligned} \mathrm{E}I_Z(u_k) &= f_Z(u_k) + o(1), \quad \textit{for } \epsilon \le u_k \le \pi, \\ \mathrm{E}I_X(u_k) &= f_X(u_k) + o(1), \quad \textit{for } \epsilon \le |u_k - \omega|,\ u_k \le \pi. \end{aligned} \tag{3.7}$$

Proof. See Appendix A of the Supplementary Material. □

THEOREM 3.2. *Let $0 < \omega < \pi$, $d \in (0, 3/2)$, and $d \ne 1/2$. Assume that the CM(ω, d) process $\{X_j\}$ satisfies Assumption 1. Then, the estimator $\widehat{\omega}$ of ω is n-consistent:*

$$|\widehat{\omega} - \omega| = O_p(n^{-1}). \tag{3.8}$$

Proof. See Appendix A of the Supplementary Material. □

Notice that the consistency result (3.8) holds both for stationary CM(ω, d) process $\{X_j\}$ when $0 < d < 1/2$ and for non-stationary process when $1/2 < d < 3/2$.

The next theorem establishes the asymptotic distribution of the estimate $\widehat{\omega}$. To describe the limit distribution, write $\widehat{\omega} = u_{\widehat{k}} = 2\pi\widehat{k}/n$, where $\widehat{k}$ is the number of the Fourier frequency that maximizes the periodogram.

THEOREM 3.3. *Assume that the CM(ω, d) process $\{X_j\}$ satisfies the assumptions of Theorem 3.2 and that (3.2) holds. Then, for any $L \ge 1$,*

$$\Pr(|\widehat{\omega} - \omega| \ge u_L) = \Pr\left(|\widehat{k} - k_0| \ge L\right) \to \Pr\left(\max_{|k| \ge L} |\tau_d(k)| > \max_{|k| < L} |\tau_d(k)|\right), \tag{3.9}$$

where the random variables $\tau_d(k)$, $k \in \mathbb{Z}$, have a known distribution which depends only on d and k.

Downloaded from https://www.cambridge.org/core. IP address: 92.41.158.104, on 12 Aug 2026 at 10:47:18, subject to the Cambridge Core terms of use, available at https://www.cambridge.org/core/terms. https://doi.org/10.1017/S0266466626100504

Proof. See Appendix A of the Supplementary Material. □

Theorem 3.3 establishes the existence of the limit distribution of the estimator $\widehat{\omega}$ providing a basis for constructing confidence intervals for ω. Similarly to the normalized periodograms of an ARFIMA process when $d \in (0, 1/2)$, see, for example, Hurvich and Beltrao (1993), the variables $\tau_d(k)$ are neither independent nor identically distributed. They are known and form a sequence of dependent random variables, the definition of which involves Gaussian sequences determined solely by the parameter d. They can be simulated, provided that d is known, and do not depend on ω or on any short-run dynamic parameters. Due to their involved structure, we do not reproduce their definitions here. Instead, we refer the reader to equations (A.41) and (A.48) in the Supplementary Material.

Building Confidence Intervals. In this article, we focus exclusively on the estimation of the parameter ω when d is unknown. Theorem 3.3 provides the basis for constructing conservative confidence intervals for ω as follows.

The researcher selects the desired coverage probability, for example, $\alpha = 0.90$ or 0.95. The confidence interval for ω is then given by

$$[\widehat{\omega} - u_m, \widehat{\omega} + u_m], \quad m = 1, 2, 3.$$

For a given m, the researcher may wish to determine the minimal level of persistence $d \geq d_{0,\alpha}^{(m)}$ required for the interval to cover ω with probability at least α. According to Theorem 3.3, these values do not depend on ω, but they do depend on m.

Simulation-based methods allow us to determine the values $d_{0,\alpha}^{(m)}$ for a range of sample sizes and values of ω (see Table 2 in Section 5). The results indicate that $d_{0,\alpha}^{(m)}$ is approximately independent of ω and n for sample sizes $n \geq 128$. Table 2 provides guidance on the coverage rate of the interval $[\widehat{\omega} - u_m, \widehat{\omega} + u_m]$ for selected values $m = 1, 2, 3$, given a user-specified lower bound for the persistence parameter d.

The width of the confidence interval is determined by the Fourier frequencies u_m. For example, to achieve 90% coverage of ω by the interval

$$[\widehat{\omega} - u_2, \widehat{\omega} + u_2],$$

that is, when ω lies within two Fourier frequencies of $\widehat{\omega}$, the minimal persistence level is approximately $d_{0,\alpha}^{(m)} \approx 0.4$ for sample sizes $n \geq 128$.

Inclusion of short-run dynamics in the ARCIMA model does not adversely affect coverage, since the spectral peak that arises from the memory parameter d dominates the contribution from shorter memory dynamics (see Figure 6 in the Supplementary Material).

Remark 3.1. In this article, we discuss cyclical processes CM(ω, d) that have a single pole in their spectrum. It can be shown that the sum $X_j = X_j(\omega_1, d_1) + \cdots + X_j(\omega_m, d_m)$ of m-mutually independent CM(ω, d) processes with parameters $(\omega_1, d_1), \ldots, (\omega_m, d_m)$ produces a time series $\{X_j\}$ with m peaks at frequencies $\omega_1, \ldots, \omega_m$ in its spectrum. We conjecture that these frequencies can be estimated

Downloaded from https://www.cambridge.org/core. IP address: 92.41.158.104, on 12 Aug 2026 at 10:47:18, subject to the Cambridge Core terms of use, available at https://www.cambridge.org/core/terms. https://doi.org/10.1017/S0266466626100504

using the frequencies $\widehat{\omega}_1,\ldots,\widehat{\omega}_m$ of the local maxima of the periodogram. These estimators have n^{-1} rate of convergence and a similar asymptotic theory should hold as for $m=1$ discussed in this article.

Remark 3.2. Definition 2.2 introduces a stationary cyclical process X_j in (2.4) that has nonzero mean μ. The periodogram $I_X(u_k)$ at Fourier frequencies u_k, $k=1,\ldots,n-1$, is shift invariant, that is, $I_X(u_k)=I_{X+\mu}(u_k)$ for any μ. Therefore, it suffices to prove the validity of the results of this article for X_j with $\mu=0$:

$$X_j=\cos(\omega j)Z_j+\sin(\omega j)Z_j', \quad j\in\mathbb{Z}. \tag{3.10}$$

Allowing for a deterministic time-varying component $\mu_j=a\cos(\omega j)+b\sin(\omega j)$, $j\in\mathbb{Z}$, in Definition 2.2 is an interesting extension for future work.

Remark 3.3. Our theoretical results are derived under the assumption that the pole ω in Definition 2.2 coincides with a Fourier frequency, that is, $\omega=u_{k_0}$. This condition can be relaxed, though such an extension would require additional technical elaboration. In the simulation study of Section 5, we assess the performance of our estimator of ω both under the baseline case $\omega=u_{k_0}$ and in the non-Fourier frequency case, $\omega=u_{k_0}+u_1/2$. The results are nearly identical in both settings (see Tables 2 and 3 in Section 5, and Tables 4 and 5 in the Supplementary Material).

4. PARAMETRIC CYCLICALLY-INTEGRATED ARCIMA MODEL

There are several stationary parametric models that allow for the estimation of cyclical patterns in the data. Among these are the ARUMA model by Anderson (1979), the GARMA model by Gray et al. (1989, 1994) and Giraitis and Leipus (1995), and the sinusoidal waveform model by Proietti and Maddanu (2024). Separately, Abadir, Distaso, and Giraitis (2011) consider a stationary and non-stationary I(d) model with trend and non-random cycles in the mean of known periodicity.

In this section, we introduce ARCIMA as an example of a parametric model that satisfies our definition of a cyclical CM(ω,d) process. By construction, it imposes a parametric fractional ARIMA structure on I(d) process Z_j in the generating equation (2.4) of CM(ω,d) model, which shifts the pole of the spectral density of the fractional ARIMA process from zero to frequency $\omega\in(0,\pi)$. The ARCIMA model makes use of the well-known properties of the ARIMA(p,d,q) process in (1.2), which allow for an easy simulation of a Gaussian ARCIMA using the Davies and Harte (1987) algorithm.

DEFINITION 4.1. *Let $\omega\in(0,\pi)$, $d\in(0,3/2)\backslash\{1/2\}$. An* ARCIMA($p,\omega,d,q$) *process $\{X_j\}$ is a* CM(ω,d) *process in (2.4) generated by an* I(d) *process* $Z_j\sim$ ARIMA(p,d,q).

Downloaded from https://www.cambridge.org/core. IP address: 92.41.158.104, on 12 Aug 2026 at 10:47:18, subject to the Cambridge Core terms of use, available at https://www.cambridge.org/core/terms. https://doi.org/10.1017/S0266466626100504

DEFINITION 4.2. *The* CI(ω,d) *model is defined as the special case of the* ARCIMA(p,ω,d,q) *model with* $p=q=0$*, that is, an* ARCIMA$(0,\omega,d,0)$ *process.*

Remark 4.1. For $0<d<1/2$, the CI(ω,d) process is covariance stationary. Its autocovariance function exhibits damped oscillations and decays to zero, while its spectral density has an infinite peak at frequency ω:

$$\gamma_X(k)=\cos(\omega k)\gamma_Z(k)=\cos(\omega k)\big(ck^{-1+2d}+o(1)\big),\quad k\to\infty, \tag{4.1}$$

$$\begin{aligned} f_X(u)&=(f_Z(u-\omega)+f_Z(u+\omega))/2,\qquad 0\le u\le\pi,\\ &=|u-\omega|^{-2d}g_X(u), \end{aligned} \tag{4.2}$$

where

$$f_Z(u)=(\sigma_\zeta^2/2\pi)|1-\mathrm{e}^{\mathrm{i}u}|^{-2d}=(\sigma_\zeta^2/2\pi)|2\sin(u/2)|^{-2d}.$$

Here, $f_Z(u)$ is the spectral density of an ARIMA$(0,d,0)$ process, and $g_X(u)=|u-\omega|^{2d}(f_Z(u-\omega)+f_Z(u+\omega))/2$ is a Lipschitz Λ_{2d} function with parameter $2d$. This holds because both $|u-\omega|^{2d}f_Z(u-\omega)$ and $f_Z(u+\omega)$ are differentiable functions on $[0,\pi]$ and $|u-\omega|^{2d}$ belongs to Λ_{2d}.

Similar asymptotic properties hold for the parametric autocorrelation function (8.1) in Abadir and Talmain (2011) and the corresponding spectrum in their Definition 8.1.

Remark 4.2. Notably, the ARCIMA and GARMA classes of cyclical models are not nested. Consider a stationary ARCIMA$(0,\omega,d,0)$ process X_j as in (2.4), generated by an ARFIMA$(0,d,0)$ process Z_j with $|d|<1/2$. Its spectral density is given by

$$\begin{aligned} f_X(d,u)&=(f_Z(u-\omega)+f_Z(u+\omega))/2,\\ f_Z(u)&=\frac{\sigma^2}{2\pi}|1-\mathrm{e}^{\mathrm{i}u}|^{-2d}=\frac{\sigma^2}{2\pi}|2\sin(u/2)|^{-2d}. \end{aligned}$$

By contrast, the GARMA$(0,d,0)$ process has spectral density

$$f_{GARMA}(u)=\frac{2\pi}{\sigma_\zeta^2}f_Z(u-\omega)f_Z(u+\omega)=\frac{\sigma_\zeta^2}{2\pi}|1-2\cos(\omega)\mathrm{e}^{\mathrm{i}u}+\mathrm{e}^{\mathrm{i}2u}|^{-2d}.$$

It is straightforward to verify that

$$\frac{2\pi}{\sigma_\zeta^2}f_{GARMA}(u)=\frac{f_X(-d,u)}{f_X(d,u)}, \tag{4.3}$$

which shows that GARMA and ARCIMA models are not nested.

Equality (4.3) demonstrates that the cyclical memory of a stationary ARCIMA time series X_j cannot be removed by GARMA-type fractional differencing. The filtered series

$$Y_j=(1-2\cos(\omega)B+B^2)^dX_j$$

Downloaded from https://www.cambridge.org/core. IP address: 92.41.158.104, on 12 Aug 2026 at 10:47:18, subject to the Cambridge Core terms of use, available at https://www.cambridge.org/core/terms. https://doi.org/10.1017/S0266466626100504

has spectral density

$$f_Y(u) = |1 - 2\cos(\omega)e^{iu} + e^{i2u}|^{2d} f_X(d, u),$$

which coincides with the spectral density $f_X(-d, u)$ of a stationary cyclical ARCIMA process with memory parameter $-d$.

It is important to point out the connection between (4.3) and Proposition 3(ii) in Proietti and Maddanu (2024). Their result establishes the relationship between ARCIMA and GARMA representations as in (2.7) for Gaussian processes, and this relation follows directly from the equality of the spectral densities in (4.3).

In terms of the GARMA model, the algorithm by Davies and Harte (1987) allows the simulation of a Gaussian version of the process, but requires knowledge of its autocovariance function, which for a GARMA$(0, d, 0)$ process is rather complicated, and not available for models with multiple poles. Further, the sharpness of the spectral peak of the GARMA model is not uniform over the location of the peak, ω, and the memory parameter d is doubled to $2d$ when $\omega \to 0$. Given that in many applications ω may be close to zero, this complicates the use of the GARMA model in empirical studies.

The generalized harmonically weighted cyclical process (GHW) introduced by Maddanu (2022) also generates peaks in the spectrum and allows for non-stationarity. This model does not include a long-memory parameter, nor does it require its estimation; however, the persistence of the GHW process again varies with the frequency parameter ω. The GHW process is universally less persistent than the GARMA process, regardless of the value of $d \in (0, 1)$. The AR(2) model with complex conjugate characteristic roots, widely used in macroeconomics, can also produce sharp finite spectral peaks at the frequency ω when the process is in the near-unit root region. Estimation of ω under either specification is challenging and requires separate investigation. Further work is also needed to develop specification tests capable of distinguishing the ARCIMA model from competing cyclical models. For alternative approaches to modeling cyclical persistence, see del Barrio Castro et al. (2024).

On the contrary, the ARCIMA model makes use of the benefits of the ARIMA framework and is much easier to simulate using the Davies and Harte (1987) algorithm. For the stationary ARIMA$(1, d, 0)$ model, the autocovariance function was derived by Hosking (1981), and for the ARIMA(p, d, q) model, explicit formulas can be found in Sowell (1992). Importantly, the persistence or sharpness of the peak in the spectrum in this specification does not vary with ω.

Estimation of the remaining parameters of the ARCIMA(p, ω, d, q) model is a challenging problem. Proietti and Maddanu (2024) introduce a maximum likelihood approach for estimating a stationary Gaussian ARCIMA model when the cyclical parameter (frequency ω) is known. Implementation of this approach requires caution, since misidentification of the pole frequency ω may result in over-parameterization, in which case the MLE procedure is not applicable. Moreover, for non-stationary ARCIMA models with $d > 1/2$, the estimator of the memory parameter often tends to hit the upper bound of the stationarity region, that is,

Downloaded from https://www.cambridge.org/core. IP address: 92.41.158.104, on 12 Aug 2026 at 10:47:18, subject to the Cambridge Core terms of use, available at https://www.cambridge.org/core/terms. https://doi.org/10.1017/S0266466626100504

$\widehat{d} \approx 1/2$. Parametric Whittle estimation of a stationary GARMA model when the frequency ω of an infinite spectral peak is unknown was investigated in Giraitis et al. (2001). Alternatively, Arteche (2020) introduced an exact local Whittle estimation method for GARMA models (both stationary and non-stationary) when the frequency ω of the spectral pole is known.

We conjecture that the same asymptotic theory established in this article also holds for the estimator $\widehat{\omega}$ of the pole location ω under a general GARMA specification. However, in this case, the variables $\tau_d(k)$, $k \in \mathbb{Z}$, appearing in the limit distribution of $\widehat{\omega}$ in Theorem 3.3, would need to be slightly modified. A formal derivation of this extension is currently work in progress.

It is worth noting that consistent estimation of d, though desired, is not necessary for the purpose of recovering ω. The confidence intervals provided in this article are conservative. Hence, so long as $\widehat{d} \geq 0.35$, we can be at least 90% confident that ω lies within two Fourier frequencies of the true pole (see Table 2). The estimation methods proposed in Proietti and Maddanu (2024) and Arteche (2020) can give some indication of the value of d of a Gaussian ARCIMA process when ω is known. An estimation procedure for the ARCIMA(p, ω, d, q) model (both stationary and non-stationary) under unknown ω is being developed and it does not reduce to a straightforward generalization of Arteche (2020).

5. MONTE CARLO SIMULATIONS

In this section, we study the finite sample properties of our estimator $\widehat{\omega}$ of the location of the cyclicality parameter ω given in (3.1).

5.1. Coverage Rates under CI(ω, d)

First, we evaluate the precision of estimation of $\omega = u_{k_0}$ by $\widehat{\omega} = u_{\widehat{k}}$ and its relation to the memory parameter d. We compute the coverage rates for confidence intervals $\widehat{\omega} \pm u_m$,

$$\Pr\left(\omega \in (\widehat{\omega} - u_m, \widehat{\omega} + u_m)\right) = \Pr(|\widehat{\omega} - \omega| \leq u_m) = \Pr(|\widehat{k} - k_0| \leq m), \quad m = 1, 2, 3;$$

the probability that ω is within one, two, or three Fourier frequencies of $\widehat{\omega}$. As $n \to \infty$, these probabilities converge to the limit coverage probabilities described by (3.9) of Theorem 3.3.

We generate 2,000 samples of the parametric Gaussian CI(ω, d) process (equivalently, ARCIMA$(0, \omega, d, 0)$), as defined in Section 4, with parameters $\omega = \left\{\frac{\pi}{4}, \frac{\pi}{8}, \frac{\pi}{16}, \frac{\pi}{32}\right\}$, $d = \{1.00, 0.50, 0.45, 0.30\}$, and for sample sizes $n = \{64, 128, 256, 512, 1{,}024\}$, using the Davies and Harte (1987) algorithm. Notice that such ω can be written as $\omega = u_{k_0}$ for some integer k_0 as required in Theorem 3.3. Table 1 shows the rate at which the true pole ω (location of peak in spectrum) falls within one, two, or three Fourier frequencies from the estimated pole $\widehat{\omega}$, see (3.1), for the values of ω, d, and n considered. It is clear that the

Downloaded from https://www.cambridge.org/core. IP address: 92.41.158.104, on 12 Aug 2026 at 10:47:18, subject to the Cambridge Core terms of use, available at https://www.cambridge.org/core/terms. https://doi.org/10.1017/S0266466626100504

TABLE 1. Coverage rate for confidence intervals $\widehat{\omega} \pm u_m$ of ω for $m = 1, 2, 3$.

ω	$d\backslash n$	64	128	256	512	1,024	64	128	256	512	1,024	64	128	256	512	1,024
				$\Pr(\lvert\widehat{k}-k_0\rvert \le 1)$					$\Pr(\lvert\widehat{k}-k_0\rvert \le 2)$					$\Pr(\lvert\widehat{k}-k_0\rvert \le 3)$		
$\frac{\pi}{4}$ (=0.785)	1.00	0.99	0.99	0.99	0.99	1.00	1.00	1.00	1.00	1.00	1.00	1.00	1.00	1.00	1.00	1.00
	0.50	0.95	0.96	0.96	0.97	0.97	0.98	0.99	0.99	0.99	0.99	0.99	0.99	1.00	1.00	1.00
	0.45	0.96	0.96	0.97	0.96	0.98	0.98	0.98	0.99	0.98	0.99	0.99	0.99	0.99	0.99	1.00
	0.30	0.69	0.72	0.76	0.76	0.79	0.78	0.79	0.83	0.86	0.87	0.83	0.84	0.88	0.90	0.90
$\frac{\pi}{8}$ (=0.393)	1.00	0.99	0.99	0.99	1.00	1.00	1.00	1.00	1.00	1.00	1.00	1.00	1.00	1.00	1.00	1.00
	0.50	0.94	0.96	0.96	0.97	0.97	0.97	0.98	0.99	0.99	0.99	0.98	0.99	0.99	1.00	1.00
	0.45	0.94	0.95	0.96	0.97	0.98	0.97	0.98	0.98	0.98	0.99	0.98	0.99	0.99	0.99	0.99
	0.30	0.69	0.71	0.73	0.76	0.78	0.79	0.78	0.81	0.84	0.86	0.86	0.84	0.86	0.88	0.89
$\frac{\pi}{16}$ (=0.196)	1.00	0.97	0.99	0.99	0.99	1.00	–	1.00	1.00	1.00	1.00	–	1.00	1.00	1.00	1.00
	0.50	0.93	0.95	0.96	0.97	0.97	–	0.98	0.98	0.99	0.99	–	0.99	0.99	1.00	1.00
	0.45	0.95	0.95	0.96	0.96	0.97	–	0.97	0.98	0.98	0.99	–	0.98	0.99	0.99	1.00
	0.30	0.70	0.68	0.71	0.73	0.77	–	0.78	0.79	0.82	0.84	–	0.85	0.84	0.86	0.88
$\frac{\pi}{32}$ (=0.098)	1.00	–	0.98	0.99	0.99	0.99	–	–	1.00	1.00	1.00	–	–	1.00	1.00	1.00
	0.50	–	0.94	0.95	0.97	0.97	–	–	0.97	0.99	0.99	–	–	0.99	0.99	0.99
	0.45	–	0.95	0.96	0.96	0.96	–	–	0.98	0.98	0.98	–	–	0.99	0.99	0.99
	0.30	–	0.70	0.68	0.70	0.71	–	–	0.79	0.79	0.79	–	–	0.87	0.85	0.84

Note: CI(ω, d) model with parameters $d = 1.00, 0.50, 0.45, 0.30$ and $\omega = \pi/4, \pi/8, \pi/16, \pi/32$. "-" indicates that the coverage interval includes zero frequency, that is, ω is not distinguishable from 0.

Downloaded from https://www.cambridge.org/core. IP address: 92.41.158.104, on 12 Aug 2026 at 10:47:18, subject to the Cambridge Core terms of use, available at https://www.cambridge.org/core/terms. https://doi.org/10.1017/S0266466626100504

coverage remains remarkably stable across ω even when it approaches zero, for sample sizes $n \geq 64$. The coverage rate depends on d and slightly drops when d decreases to 0.3. Otherwise, for $d \geq 0.45$, the interval $(\widehat{\omega} - u_1, \widehat{\omega} + u_1)$ produces $\geq$95% coverage for ω. The stability of this (conservative) coverage rate suggests that, in practice, a prominent peak in the periodogram which represents cyclical patterns with memory parameter $d \geq 0.35$ can be viewed as a very accurate estimate of ω irrespective where it is located. This experiment confirms the theoretical findings of Theorem 3.3.

5.2. Setup for More General Models

Next, in order to verify our theoretical findings, we consider the following non-trended CI(ω, d), trending CI(ω, d), and de-trended CI(ω, d) models. We use them to generate data samples of cyclical processes with a pole at frequency ω in their spectrum and characterized by integration parameter d:

$$\text{CI}(\omega, d) \text{ model}: \; X_t = \cos(\omega t) Z_t + \sin(\omega t) Z_t', \tag{5.1}$$

$$\text{Trending CI}(\omega, d) \text{ model}: \; Y_t = \mu + \beta t + X_t, \quad X_t \sim \text{CI}(\omega, d),$$
$$\text{De-trended CI}(\omega, d) \text{ model}: \; \widetilde{X}_t = Y_t - \widehat{\mu} - \widehat{\beta} t, \tag{5.2}$$

where $\{Z_t\}$ and $\{Z_t'\}$ are independent fractional ARIMA$(0, d, 0)$ processes, $\mu = \beta = 1$, and $\widehat{\mu}$, $\widehat{\beta}$ are the OLS estimates of μ and β.

We generate samples of CI models (5.1) and (5.2) with parameter ω taking values at Fourier frequencies $\omega = u_{k_0} = 2\pi k_0/n$, for $k_0 = \{8, 16, 32, 64, 128\}$ and sample sizes $n = \{64, 128, 256, 512, 1024\}$. We use $0 < d \leq 1$ and run Monte Carlo experiments over 2,000 replications. We also examine CI(ω, d) models with parameter $\omega = u_{k_0} + u_1/2$ which does not coincide with a Fourier frequency.

5.3. Results for More General Models

We commence with a visualization of data plots, sample auto-correlation functions (ACFs), and periodograms of the cyclically integrated CI(ω, d) process with spectral density that has a pole at the frequency $\omega = \pi/16$ corresponding to u_{k_0} with $k_0 = 16$ and $n = 512$. Note that the definition of the sample ACFs plotted here is $\widehat{\gamma}_X(k)/\widehat{\gamma}_X(0)$ (cf. the generalized version of ACFs in Abadir, Caggiano, and Talmain, 2013).

Figure 1 displays plots of two CI processes and their corresponding ACFs and periodograms for: (i) $d = 0.45$ (the stationary $\{X_j\}$ is a cyclical long-memory process) and (ii) $d = 1$ (the non-stationary $\{X_j\}$ is a cyclical unit-root process). The cyclicality in the realization is more pronounced when $d = 1$. While the shapes of the ACFs are similar, the range of ACF is wider under the unit root setting ($d = 1$). Notably, the peak of the periodogram at frequency $\omega = \pi/16$ is disproportionately sharper for the cyclical unit root (with $d = 1$) when compared to stationary long-memory process (with $d = 0.45$).

Downloaded from https://www.cambridge.org/core. IP address: 92.41.158.104, on 12 Aug 2026 at 10:47:18, subject to the Cambridge Core terms of use, available at https://www.cambridge.org/core/terms. https://doi.org/10.1017/S0266466626100504

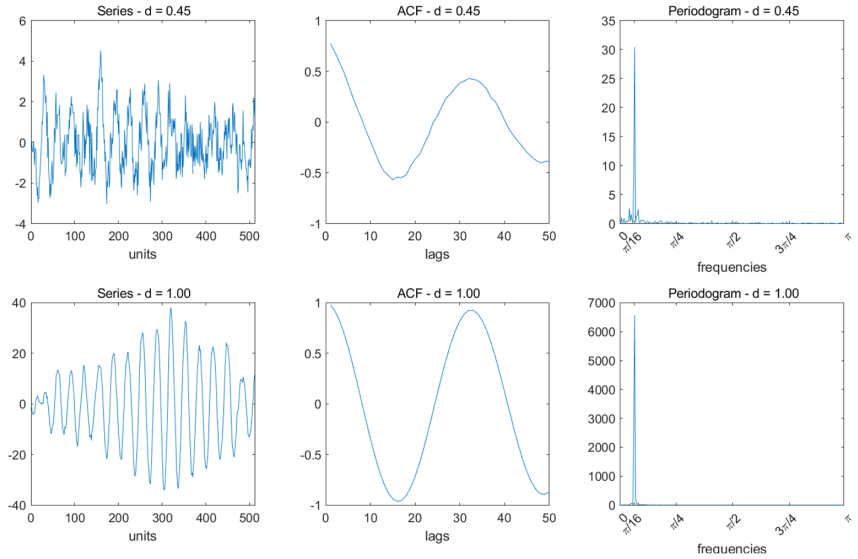


FIGURE 1. CI(ω, d) process: plots, ACFs, and periodograms.
Note: CI(ω, d) generated by model (5.1) with $\omega = \pi/16$ and $d = \{0.45, 1\}$. Sample size $n = 512$.

Figure 2 depicts plots, ACFs, and periodograms of a trending CI(ω, d) process and its de-trended version (5.2) when $\omega = \pi/16$ and $d = 0.45$. For the trending series, cyclicality inherent in CI is still evident but now the series oscillates around its trend, and the ACF decays slowly in an almost linear fashion.

Clearly, the cyclical peak in the periodogram at $\omega = \pi/16$ is overshadowed by the spike in the periodogram at zero frequency due to the linear trend, a permanent component which has not been removed from the series. Once de-trended, the plot of the data, ACF, and periodogram resemble more those of the original stationary CI series with $d = 0.45$.

From Figures 1 and 2, it is evident that the peak in the periodogram of the CI(ω, d) model becomes more pronounced when d increases. In Table 2, we assess the probability $\Pr\left(\omega \in [\widehat{\omega} \pm u_m]\right) = \Pr\left(|\widehat{k} - k_0| \leq m\right)$ that the unknown ω is within one, two, or three Fourier frequencies of $\widehat{\omega}$. In particular, it reports for a given m, the range of memory parameters $d \geq d_{0,\alpha}$ for which coverage is larger than $\alpha = 0.9$ or 0.95. The lower bound $d_{0,\alpha}$ for d, that guarantees 90% and 95% coverage, seems to be approximately the same across ω for $n \geq 128$, which is in line with the theory. We observe that $d_{0,\alpha}$ does not depend on the values $\omega = \frac{\pi}{4}, \frac{\pi}{8}, \frac{\pi}{16}$ and sample sizes $n = 128, 256, 512, 1,024$. For example, for $\omega = \pi/4$ and $n = 125, 256, 512, 1,024$, the table indicates that $\Pr\left(\omega \in [\widehat{\omega} \pm u_3]\right) \geq 0.9$ for $d \geq 0.35$ and $\Pr\left(\omega \in [\widehat{\omega} \pm u_1]\right) \geq 0.95$ for $d \geq 0.45$. In turn, $d_{0,\alpha}$ becomes slightly larger when the sample size is small, $n = 64$.

Downloaded from https://www.cambridge.org/core. IP address: 92.41.158.104, on 12 Aug 2026 at 10:47:18, subject to the Cambridge Core terms of use, available at https://www.cambridge.org/core/terms. https://doi.org/10.1017/S0266466626100504

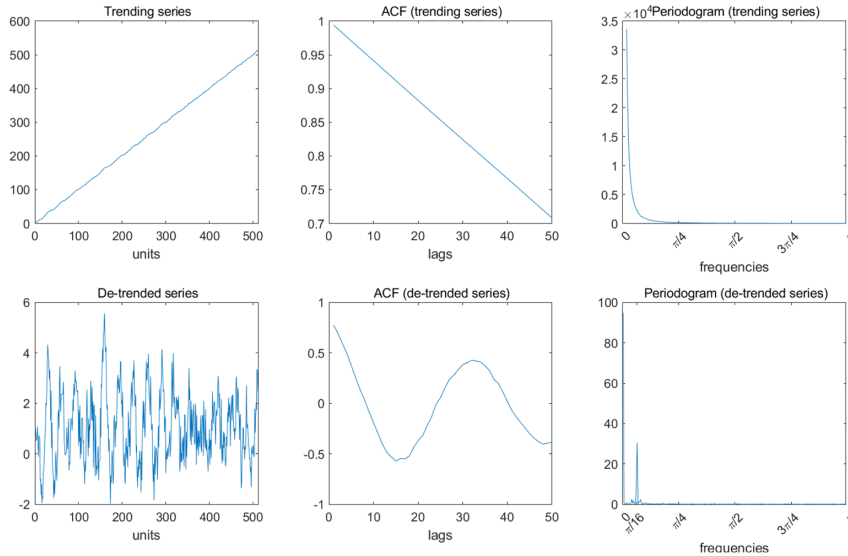


FIGURE 2. Trending and de-trended CI(ω, d) process: plots, ACFs, and periodograms.
Note: Trending and de-trended CI(ω, d) process generated by model (5.2) with $\omega = \pi/16$ and $d = 0.45$. Sample size $n = 512$.

Table 3 reports results for the de-trended CI(ω, d) model. They are comparable to those in Table 2 as long as sample sizes are not too small (e.g., $n \geq 256$).

Shifting the pole at $\omega = u_{k_0}$ to a non-Fourier frequency $\omega = u_{k_0} + u_1/2$ produces nearly identical results to the baseline scenarios analyzed in Tables 2 and 3 (see Tables 4 and 5 in the Supplementary Material).

Overall, the Monte Carlo study confirms that the estimator $\widehat{\omega}$ captures the frequency ω effectively when d is relatively large, ($d \geq 0.4$), and thus when the peak in the spectrum and periodogram is more pronounced. This can be useful in practice, when attempting to identify unknown pronounced cyclical patterns, such as business cycle effects, with confidence.

6. EMPIRICAL ILLUSTRATION

Many time series display (quasi-)periodic behavior at different frequencies. Examples in economics include macroeconomic time series, such as GDP or IP, which are typically used in the analysis of business cycles (see Harvey and Jaeger, 1993 and Kulish and Pagan, 2021, among others). Examples in climate research cover paleoclimatic data, such as global land–ocean temperature (GLOTI), methane (CH_4), and carbon dioxide (CO_2) concentration, ice volume (see McElroy and Politis, 2024, Proietti and Maddanu, 2024, and references therein). In our empirical illustration, we focus on discerning frequencies at which peaks in the spectrum

Downloaded from https://www.cambridge.org/core. IP address: 92.41.158.104, on 12 Aug 2026 at 10:47:18, subject to the Cambridge Core terms of use, available at https://www.cambridge.org/core/terms. https://doi.org/10.1017/S0266466626100504

TABLE 2. Minimum value $d_{0,\alpha}$ of parameter d in CI(ω, d) model such that ω is contained in $\widehat{\omega} \pm u_m$, $m = 1, 2, 3$ with probability $\alpha = 0.9, 0.95$ when $d \geq d_{0,\alpha}$.

ω	α	$n =$	64	128	256	512	1,024	64	128	256	512	1,024	64	128	256	512	1,024
			$\Pr(\widehat{k} - k_0 \leq 1) \geqslant \alpha$					$\Pr(\widehat{k} - k_0 \leq 2) \geqslant \alpha$					$\Pr(\widehat{k} - k_0 \leq 3) \geqslant \alpha$				
$\frac{\pi}{4}$	0.90	for $d \geq$	0.45	0.40	0.40	0.40	0.40	0.40	0.40	0.35	0.35	0.35	0.35	0.35	0.35	0.35	0.30
	0.95		0.45	0.45	0.45	0.45	0.45	0.45	0.45	0.40	0.40	0.40	0.40	0.40	0.40	0.40	0.35
$\frac{\pi}{8}$	0.90		0.45	0.45	0.40	0.40	0.40	0.40	0.40	0.40	0.35	0.35	0.35	0.35	0.35	0.35	0.35
	0.95		0.60	0.45	0.45	0.45	0.45	0.45	0.45	0.45	0.40	0.40	0.40	0.40	0.40	0.40	0.35
$\frac{\pi}{16}$	0.90		0.45	0.45	0.45	0.40	0.40	0.35	0.40	0.40	0.35	0.35	0.35	0.35	0.35	0.35	0.35
	0.95		0.70	0.55	0.45	0.45	0.45	0.40	0.45	0.45	0.40	0.40	0.40	0.40	0.40	0.40	0.40

Note: CI(ω, d) in (5.1). Number of replications 2,000.

Downloaded from https://www.cambridge.org/core. IP address: 92.41.158.104, on 12 Aug 2026 at 10:47:18, subject to the Cambridge Core terms of use, available at https://www.cambridge.org/core/terms. https://doi.org/10.1017/S0266466626100504

TABLE 3. Minimum value $d_{0,\alpha}$ of parameter d in de-trended CI(ω, d) model such that ω is contained in $\widehat{\omega} \pm u_m$, $m = 1, 2, 3$ with probability $\alpha = 0.9, 0.95$ when $d \geq d_{0,\alpha}$.

ω	α	$n =$	64	128	256	512	1,024	64	128	256	512	1,024	64	128	256	512	1,024
			$\Pr(\lvert\widehat{k} - k_0\rvert \leq 1) \geqslant \alpha$					$\Pr(\lvert\widehat{k} - k_0\rvert \leq 2) \geqslant \alpha$					$\Pr(\lvert\widehat{k} - k_0\rvert \leq 3) \geqslant \alpha$				
$\frac{\pi}{4}$	0.90	for $d \geq$	0.45	0.45	0.40	0.40	0.40	0.45	0.40	0.40	0.35	0.35	0.45	0.40	0.35	0.35	0.35
	0.95		0.70	0.45	0.45	0.45	0.45	0.60	0.45	0.45	0.40	0.40	0.60	0.45	0.40	0.40	0.35
$\frac{\pi}{8}$	0.90		0.75	0.45	0.45	0.40	0.40	0.70	0.45	0.40	0.40	0.35	0.70	0.45	0.40	0.35	0.35
	0.95		0.95	0.70	0.50	0.45	0.45	0.85	0.55	0.45	0.45	0.40	0.85	0.55	0.45	0.40	0.40
$\frac{\pi}{16}$	0.90		–	0.75	0.45	0.45	0.40	0.35	0.70	0.45	0.40	0.40	0.30	0.70	0.45	0.40	0.35
	0.95		–	0.90	0.65	0.50	0.45	0.40	0.90	0.50	0.45	0.45	0.35	0.90	0.50	0.45	0.40

Note: De-trended CI(ω, d) in (5.2). "-" indicates that confidence interval for ω includes 0. 2,000 replications.

Downloaded from https://www.cambridge.org/core. IP address: 92.41.158.104, on 12 Aug 2026 at 10:47:18, subject to the Cambridge Core terms of use, available at https://www.cambridge.org/core/terms. https://doi.org/10.1017/S0266466626100504

are evident for: (i) U.S. nominal GDP over the period Q1-1956 to Q4-2019,[2] (ii) U.S. real IP over the period August 1977 to December 2019,[3] and (iii) CO_2 concentration (CO_2) over the period May 1978 to December 2020,[4] using our estimator introduced in Section 3.

6.1. U.S. Nominal GDP

We start with the analysis of cyclical patterns in quarterly U.S. nominal GDP which is one of the broadest measures of economic activity. A major subfield of macroeconomics focuses on the discovery and extraction of long cycles such as the 2–8 year business cycle, as these convey important information for use when implementing policy adjustments to economic shocks.

Two main considerations in the analysis of business cycles are the choices of (i) seasonal and (ii) "trend" filtering to be applied to the original time series. In (i), adjustment of the raw data from seasonal effects (that are assumed known) typically precedes the analysis of any remaining (unknown) quasi-periodic cycles and is based on linear filtering. One of the most prominent filtering methods is X-12-ARIMA developed by the U.S. Bureau of Census (see Findley et al., 1998). With respect to the "trend" filtering (ii), a number of filters have been considered, such as Hodrick and Prescott (1997), Baxter and King (1999), Christiano and Fitzgerald (2003), and Beveridge and Nelson (1981). These filters differ from each other in terms of the assumed type of "trend" present in the original data and dependence assigned to the transformed data. However, as argued in Harvey and Jaeger (1993), Ghysels, Granger, and Siklos (1996), and more recently Kulish and Pagan (2021), use of inappropriate seasonal adjustment and de-trending techniques can lead investigators to report spurious cyclical behavior. More recent contributions allow for the possibility of more flexible fractional differencing where d is non-integer and resides in both the stationary and non-stationary domain (see Hart and Jucknewitz, 2022).

We focus on non-seasonally adjusted U.S. nominal GDP to investigate the existence of persistent long cycles in order to circumvent distorting effects arising from seasonal filtering. Figure 3 (top left panel) depicts the logarithmic transformation $\log(GDP)$ of the data where repeated oscillations of different lengths are evident.[5] In the frequency domain, a large peak of the periodogram at zero frequency dominates over any additional spectral mass at other nonzero frequencies (see

[2]The quarterly non-seasonally adjusted (nsa) nominal Gross Domestic Product, USD billions, is obtained from the Bureau of Economic Analysis (https://www.bea.gov/).

[3]The monthly non-seasonally adjusted (nsa) real total IP index, 2017=100, is obtained from the Federal Reserve Economic Database of the Federal Reserve Bank of St. Louis (https://fred.stlouisfed.org).

[4]The monthly atmospheric carbon dioxide series consists of CO_2 concentration measurements in parts per million (ppm) collected at the summit of Mauna Loa mountain in Hawaii. Source: National Oceanographic and Atmospheric Administration Climate Monitoring and Diagnostics Laboratory, and Keeling et al. (1976).

[5]The original nsa nominal GDP series extends back to Q1-1947 and ends in Q2-2023. We adjusted its length to achieve a sample size of $256 = 2^8$ and to exclude the COVID-19 disruption which would have required an addition to the model.

Downloaded from https://www.cambridge.org/core. IP address: 92.41.158.104, on 12 Aug 2026 at 10:47:18, subject to the Cambridge Core terms of use, available at https://www.cambridge.org/core/terms. https://doi.org/10.1017/S0266466626100504

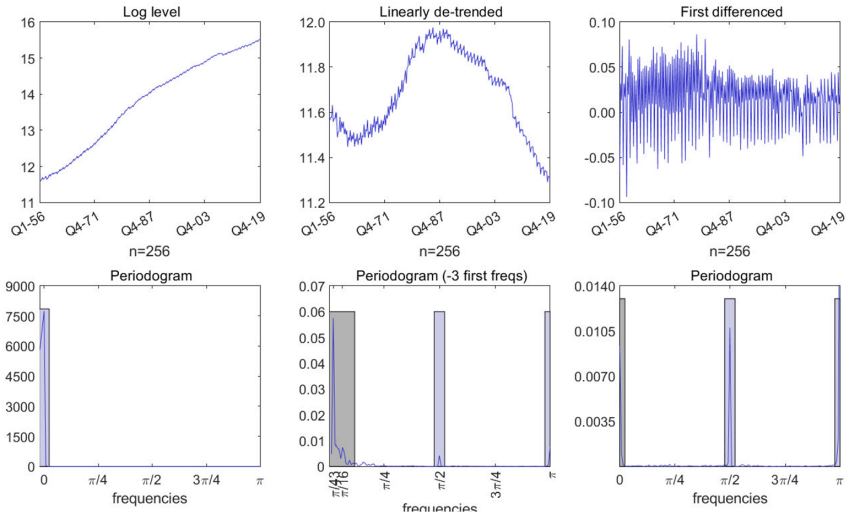


FIGURE 3. Plots of log transformed, linearly de-trended, and first differenced U.S. non-seasonally adjusted nominal GDP (Q1 1956–Q4 2019), and corresponding periodograms.

Note: Shaded areas are drawn across three frequencies on either side of each peak in the respective periodograms.

Figure 3 [bottom left panel]). Using the ACF domain approach, the properties of this series were analyzed by Abadir et al. (2013) and their tests rejected the ARIMA-type non-cyclical model in favor of the parametric cyclical model considered in their work.

The periodogram of the linearly de-trended $\log(GDP)$ series more clearly uncovers the existence of one or more long cycles in the level of nominal GDP, in addition to typical seasonal variations (see Figure 3 [top and bottom middle panels]).[6] First, clearly-defined peaks are evident at the two seasonal frequencies $\pi/2$ and π (shaded light purple areas),[7] which coincide with annual and semi-annual cycles, respectively. We also distinguish a mass at the lower frequency of $\pi/43$ (shaded light gray area). The length of the corresponding cycle, $\widehat{\lambda} = 2\pi/\widehat{\omega}$, equates to 21.3 years, indicative of the longer cycle also found in the analysis of Abadir et al. (2013)—see their Figure 2. Additional mass can be detected at close-by frequencies, such as at frequency $\pi/16$, which translates into a cycle of eight

[6]Upon de-trending, a substantial peak is still evident at zero frequency of the corresponding periodogram, though it is less pronounced than in Figure 3 (bottom left panel). For this reason, in the plot, we disregard the first three Fourier frequencies ($k = 0, 1, 2$). See also Bailey and Giraitis (2016) on the sufficient (finite) number of frequencies around zero required to describe persistent time dependence. Investigation of the appropriate de-trending approach to be used is beyond the scope of this article. We refer the reader to Hart and Jucknewitz (2022) and references therein on this issue.

[7]The shaded areas are drawn across three frequencies on either side of each peak (i.e., across seven frequencies overall) for visual clarity.

Downloaded from https://www.cambridge.org/core. IP address: 92.41.158.104, on 12 Aug 2026 at 10:47:18, subject to the Cambridge Core terms of use, available at https://www.cambridge.org/core/terms. https://doi.org/10.1017/S0266466626100504

years, the upper bound of the range associated with the business cycle. Overall, without imposing further adjustments to this GDP process, we can infer with confidence that persistent seasonal patterns are evident and well-captured by our estimator, while deciphering distinct longer cycles by means of the periodogram is more ambiguous and requires a more finely-tuned analysis.

Focusing on growth rates in nominal GDP (first-differenced $\log(GDP)$) instead, produces a periodogram that has significant peaks at the same seasonal frequencies $\pi/2$ and π, but provides a less detailed account of potential cyclical behavior at frequencies close to zero (see Figure 3 [top and bottom right panels]).

6.2. U.S. Real Industrial Production

Turning to the real economy, we also consider the analysis of (quasi-)periodic patterns in U.S. IP which is recorded at a higher frequency (monthly) and focuses on economic activity in the industrial sector (see Ghysels, 1997; A'Hearn and Woitek, 2001). As before, we are interested in non-seasonally adjusted U.S. real IP.

Figure 4 (top left panel) plots IP in log levels, $\log(IP)$, where we distinguish regular oscillations of different periods.[8] This series shows clear signs of significant persistence when looking at the large peak at zero frequency in its corresponding periodogram (bottom left panel of Figure 4). Any signs of additional structure linked to cycles at frequencies away from zero are dominated by the "trend" component, as in the case of nominal GDP.

To uncover other peaks in the periodogram, we apply linear de-trending and alternatively first differencing to $\log(IP)$ (see Figure 4 [top middle and right panels, respectively]). The corresponding periodograms are depicted in the bottom middle and right panels of Figure 4. In both cases, our estimator identifies substantial mass (peaks) at the seasonal frequencies ω, $\left\{\frac{\pi}{6}, \frac{\pi}{3}, \frac{\pi}{2}, \frac{2\pi}{3}, \frac{5\pi}{4.5}, \pi\right\}$ (shaded light purple areas),[9] which coincide with cycles of length $\{12, 6, 4, 3, 2.4, 2\}$ months, respectively. Given that seasonal fluctuations are very regular and consistent, it is expected that the peaks at these frequencies are well defined. However, their memory parameters, d's, are not guaranteed to be uniformly equal to unity (seasonal unit root) which is the typical assumption made in seasonal adjustment methods. Interestingly, we can also distinguish mass at the lower frequency of $\pi/20$ (shaded light gray area) which, depending on the focus on level or growth rates of real IP, appears more or less pronounced than those attached to seasonal peaks. The length of the corresponding cycle, $\widehat{\lambda} = 2\pi/\widehat{\omega}$, equates to 3.3 years and falls within the 2–8 year bounds assigned to the business cycle. What is evident in both cases is that this mass is not as clearly defined as those at the seasonal

[8]The original nsa IP series extends back to January 1919 and ends in August 2023. We adjusted its length to achieve a sample size of $512 = 2^9$ and to exclude the disruptions from the Great Depression and COVID-19.

[9]The shaded areas are drawn across three frequencies on either side of each peak (i.e., across seven frequencies overall) for visual clarity.

Downloaded from https://www.cambridge.org/core. IP address: 92.41.158.104, on 12 Aug 2026 at 10:47:18, subject to the Cambridge Core terms of use, available at https://www.cambridge.org/core/terms. https://doi.org/10.1017/S0266466626100504

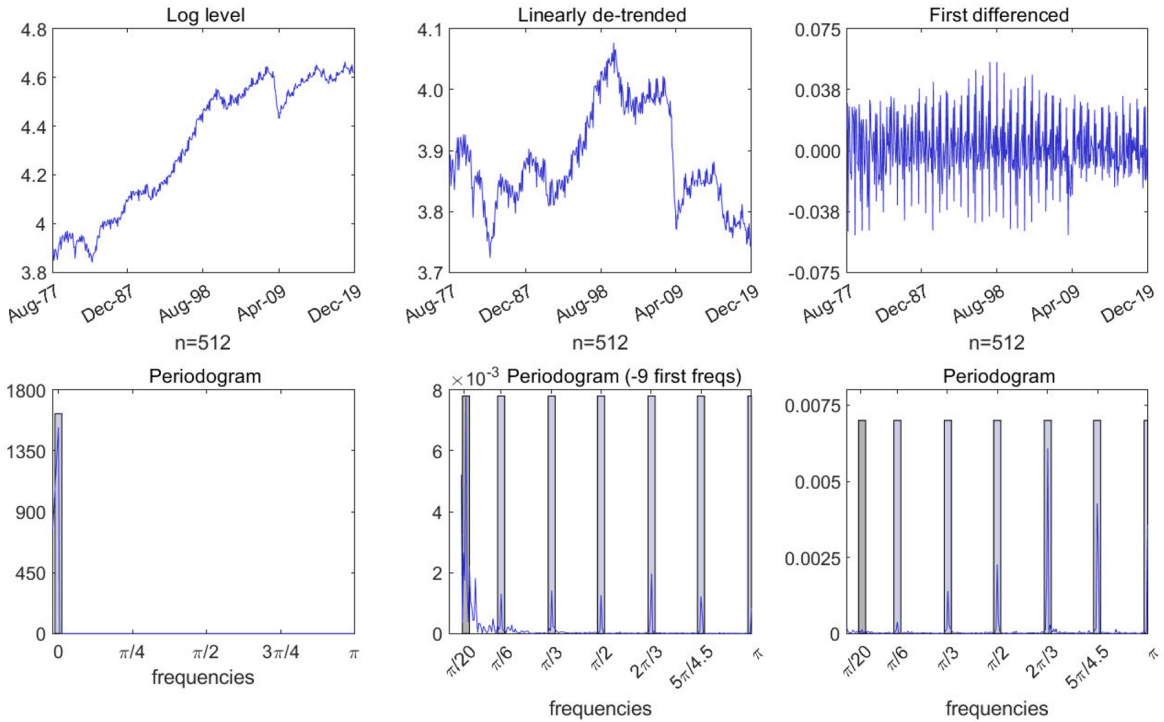


FIGURE 4. Plots of log transformed, linearly de-trended, and first differenced U.S. non-seasonally adjusted real industrial production (August 1977–December 2019), and corresponding periodograms.
Note: Shaded areas are drawn across three frequencies on either side of each peak in the respective periodograms.

Downloaded from https://www.cambridge.org/core. IP address: 92.41.158.104, on 12 Aug 2026 at 10:47:18, subject to the Cambridge Core terms of use, available at https://www.cambridge.org/core/terms. https://doi.org/10.1017/S0266466626100504

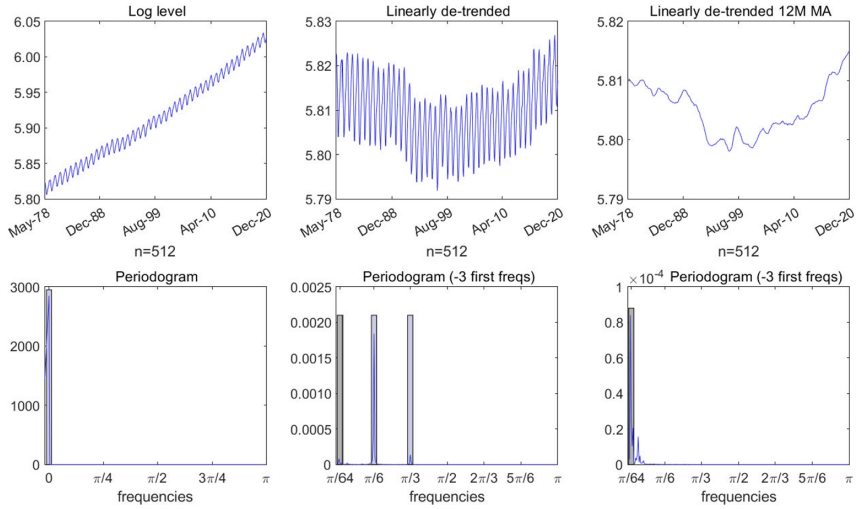


FIGURE 5. Plots of log transformed, linearly de-trended, and linearly de-trended 12-month moving average CO_2 concentration (May 1978–December 2020), and corresponding periodograms.
Note: Shaded areas are drawn across three frequencies on either side of each peak in the respective periodograms.

frequencies and thus inferring with confidence the existence and persistence of this long cycle requires additional investigation beyond the periodogram.

6.3. CO_2 Concentration

Next, we analyze CO_2 concentration which is instrumental in climate change debates, given its long history. Its monthly series is known to exhibit sawtooth patterns.[10] The same series was used in the empirical study of Proietti and Maddanu (2024) which modeled it as a compound of a linear and quadratic trend, an AR(1) process, and six periodic CM-type cycles at predetermined frequencies, $\omega_j = \frac{\pi}{6}j$, for $j = 1, 2, \ldots, 6$.

The log of the series is depicted in the top left panel of Figure 5. The plot encompasses clearly-defined and repeated oscillations over time. A large peak is evident in the periodogram of $\log(CO_2)$ at zero frequency (bottom left panel of Figure 5). Any signs of peaks at frequencies away from zero are dominated by the mass at $\omega_0 = 0$.

We apply linear de-trending to $\log(CO_2)$ and compute its corresponding periodogram. These are depicted in the top and bottom middle panels of Figure 5, respectively. There is still evidence of a sizeable peak at zero frequency, so again we disregard the first three Fourier frequencies ($k = \{0, 1, 2\}$) and focus our

[10]The monthly time series that we obtained extends back to November 1975. Its original version begins in January 1958. We adjusted its length to achieve a sample size of $512 = 2^9$.

Downloaded from https://www.cambridge.org/core. IP address: 92.41.158.104, on 12 Aug 2026 at 10:47:18, subject to the Cambridge Core terms of use, available at https://www.cambridge.org/core/terms. https://doi.org/10.1017/S0266466626100504

attention on the spectral mass in the remainder of the periodogram. Significant peaks are now revealed at periodic frequencies $\omega_1 = \frac{\pi}{6}$ and $\omega_2 = \frac{\pi}{3}$ (shaded light purple areas), which coincide with stochastic cycles of length 12 and 6 months, respectively. The theoretical results of Sections 2 and 3 indicate that the prominence of these peaks can be translated into memory parameters d_1 and d_2, in excess of 0.3 when assuming a multi-pole CM model. All potential remaining seasonal cycles must be of limited persistency and thus indistinguishable.[11]

Proietti and Maddanu (2024) proceed to estimate d_j's corresponding to frequencies $\omega_j = \frac{\pi}{6}j$, $j = 1, \ldots, 6$, over the period January 1958 to June 2020 ($n = 750$), based on a stationary ARCIMA model with $d < 0.5$. Using Maximum Likelihood, they find that $\widehat{d}_1 = 0.4995$ and $\widehat{d}_2 = 0.4980$ when $\omega_1 = \frac{\pi}{6}$ and $\omega_2 = \frac{\pi}{3}$, respectively, while $\widehat{d}_5 = 0.0569$ when $\omega_5 = \frac{5\pi}{6}$. In line with our analysis, persistent patterns at frequencies $\omega_1 = \frac{\pi}{6}$ and $\omega_2 = \frac{\pi}{3}$ should be accounted for in the modeling of CO_2 concentration but not at $\omega_5 = \frac{5\pi}{6}$. Proietti and Maddanu (2024) also conclude that $\widehat{d}_3$, $\widehat{d}_4$, and $\widehat{d}_6$ corresponding to $\omega_3 = \frac{\pi}{2}$, $\omega_4 = \frac{2\pi}{3}$, and $\omega_6 = \pi$ hit the upper bound of 0.5. In contrast, our estimator $\widehat{\omega}$ suggests that no important cycles at these frequencies can be identified and hence the need to include cyclical patterns at $\omega_3 = \frac{\pi}{2}$, $\omega_4 = \frac{2\pi}{3}$, and $\omega_6 = \pi$ in the modeling of CO_2 concentration is debatable.

Separately, from Figure 5 (bottom middle panel), we can distinguish spectral mass at the additional lower frequency, $\frac{\pi}{64}$, which could correspond to the "red noise" component discussed in Proietti and Maddanu (2024). This translates into a cycle of length of 10.7 years. The additional spectral structure becomes more evident when we model the sawtooth profile of the series: applying a simple (i.e., equal-weight) MA(12) to the de-trended $\log(CO_2)$ monthly series, we get the top and bottom right panels of Figure 5.

Overall, whether applying an estimation procedure for the memory parameters that permits for $d > 0.5$ for the cycles identified by our method produces different estimation results to those shown in Proietti and Maddanu (2024) is an open question. This exercise is beyond the scope of our article and is left for future research.

7. CONCLUSION

In this article, we introduce a class of models which allows for the modeling of persistent cyclical patterns in stationary and non-stationary time series. We show that the cyclicality parameter ω, which is represented by the location of an infinite peak in the spectrum of the time series, can be effectively estimated by maximizing the corresponding periodogram over Fourier frequencies. Theoretical results of this article allow to build confidence intervals for ω. Natural extensions to this work include the development of parameter estimation theory for the ARCIMA

[11] We also applied linear and quadratic de-trending to $\log(CO_2)$, as in Proietti and Maddanu (2024). The resulting periodogram revealed peaks at the same periodic frequencies of $\omega_1 = \pi/6$ and $\omega_2 = \pi/3$.

Downloaded from https://www.cambridge.org/core. IP address: 92.41.158.104, on 12 Aug 2026 at 10:47:18, subject to the Cambridge Core terms of use, available at https://www.cambridge.org/core/terms. https://doi.org/10.1017/S0266466626100504

model, and formal extension of the modeling to allow for a finite number of infinite peaks in the spectrum.

SUPPLEMENTARY MATERIAL

The supplementary material for this article can be found at https://doi.org/10.1017/S0266466626100504.

FUNDING STATEMENT

This work was supported by the ESRC under Grant RES062230790.

COMPETING INTERESTS

The authors declare that no competing interests exist.

REFERENCES

Abadir, K. M., Caggiano, G., & Talmain, G. (2013). Nelson-Plosser revisited: The ACF approach. *Journal of Econometrics*, 175(1), 22–34.

Abadir, K. M., Distaso, W., & Giraitis, L. (2011). An I(d) model with trend and cycles. *Journal of Econometrics*, 163(2), 186–199.

Abadir, K. M., & Talmain, G. (2002). Aggregation, persistence and volatility in a macro model. *Review of Economic Studies*, 69(4), 749–779.

Abadir, K. M., & Talmain, G. (2011). The unconventional dynamics of economic and financial aggregates. In Ullah A., and D. E. A. Giles (eds.), *Handbook of Empirical Economics and Finance* (pp. 205–213). Chapman & Hall/CRC.

A'Hearn, B., & Woitek, U. (2001). More international evidence on the historical properties of business cycles. *Journal of Monetary Economics*, 47(2), 321–346.

Andel, J. (1986). Long memory time series models. *Kybernetika*, 22(2), 105–123.

Anderson, O. D. (1979). The autocovariance structures associated with general unit circle nonstationary factors in the autoregressive operators of otherwise stationary ARMA time series models. *Cahiers du CERO*, 21, 221–237.

Arteche, J. (2020). Exact local Whittle estimation in long memory time series with multiple poles. *Econometric Theory*, 36, 1064–1098.

Bailey, N., & Giraitis, L. (2016). Spectral approach to parameter-free unit root testing. *Computational Statistics and Data Analysis*, 100, 4–16.

Baxter, M., & King, R. G. (1999). Measuring business cycles: Approximate band-pass filters for economic time series. *The Review of Economics and Statistics*, 81(4), 575–593.

Beveridge, S., & Nelson, C. R. (1981). A new approach to the decomposition of economic time series into permanent and transitory components with particular attention to measurement of the 'business cycle'. *Journal of Monetary Economics*, 7(2), 151–174.

Christiano, L., & Fitzgerald, T. J. (2003). The band pass filter. *International Economic Review*, 44(2), 435–465.

Davies, R. B., & Harte, D. S. (1987). Tests for Hurst effect. *Biometrika*, 74(1), 95–101.

del Barrio Castro, T., & Osborn, D. R. (2024). *Periodic integration and seasonal unit roots*. Oxford University Press. https://doi.org/10.1093/acrefore/9780190625979.013.665

del Barrio Castro, T., Cubadda, G., & Osborn, D. R. (2022). On cointegration for processes integrated at different frequencies. *Journal of Time Series Analysis*, 43, 412–435.

Downloaded from https://www.cambridge.org/core. IP address: 92.41.158.104, on 12 Aug 2026 at 10:47:18, subject to the Cambridge Core terms of use, available at https://www.cambridge.org/core/terms. https://doi.org/10.1017/S0266466626100504

del Barrio Castro, T., Rodrigues, P. M. M., & Taylor, A. M. R. (2018). Semi-parametric seasonal unit root tests. *Econometric Theory*, 34, 447–476.

del Barrio Castro, T., Rodrigues, P. M. M., & Taylor, A. M. R. (2019). Temporal aggregation of seasonally near-integrated processes. *Journal of Time Series Analysis*, 40, 873–886.

Findley, D. F., Monsell, B. C., Otto, W. R., & Chen, B. C. (1998). New capabilities and methods of the X-12-ARIMA seasonal-adjustment program. *Journal of Business & Economic Statistics*, 16(2), 127–152.

Frisch, R. (1933). Propagation problems and impulse problems in dynamic economics. In Kock K. (ed.), *Reprinted in: Economic essays in honor of Gustav Cassel* (p. 202). George Allen & Unwin Ltd.

Ghysels, E. (1997). Seasonal adjustment and other data transformations. *Journal of Business & Economic Statistics*, 14(4), 410–418.

Ghysels, E., Granger, C. W. J., & Siklos, P. L. (1996). Is seasonal adjustment a linear or nonlinear data-filtering process? *Journal of Business & Economic Statistics*, 14(3), 374–386.

Giraitis, L., Hildago, J., & Robinson, P. M. (2001). Gaussian estimation of parametric spectral density with unknown pole. *Annals of Statistics*, 29(4), 987–1023.

Giraitis, L., Koul, H. L., & Surgailis, D. (2012). *Large sample inference for long memory processes*. Imperial College Press.

Giraitis, L., & Leipus, R. (1995). A generalized fractionally differencing approach in long-memory modeling. *Lithuanian Mathematical Journal*, 35, 53–65.

Granger, C. W. J., & Joyeux, R. (1980). An introduction to long-memory time series models and fractional differencing. *Journal of Time Series Analysis*, 1, 15–29.

Gray, H., Zhang, N., & Woodward, W. (1989). On generalized fractional processes. *Journal of Time Series Analysis*, 10(3), 233–257.

Gray, H., Zhang, N., & Woodward, W. (1994). On generalized fractional processes—A correction. *Journal of Time Series Analysis*, 15(5), 561–562.

Hart, T., & Jucknewitz, K. (2022). Approximate state space modelling of unobserved fractional components. *Econometric Reviews*, 41(1), 75–98.

Harvey, A. C., & Jaeger, A. (1993). Detrending, stylised facts and the business cycle. *Journal of Applied Econometrics*, 8(3), 231–247.

Hidalgo, J., & Soulier, P. (2004). Estimation of the location and exponent of the spectral singularity of a long memory process. *Journal of Time Series Analysis*, 25(1), 55–81.

Hodrick, R. J., & Prescott, E. C. (1997). Postwar U.S. business cycles: An empirical investigation. *Journal of Money, Credit, and Banking*, 29(1), 1–16.

Hosking, J. R. M. (1981). Fractional differencing. *Biometrika*, 68(1), 165–176.

Hurvich, C. H., & Beltrao, K. (1993). Asymptotics for the low-frequency ordinates of the periodogram of a long-memory time series. *Journal of Time Series Analysis*, 14(5), 455–472.

Kang, D. N., & Marmer, V. (2024). Modeling long cycles. *Journal of Econometrics*, 242, 105751.

Keeling, C. D., Bacastow, R. B., Bainbridge, A. E., EkdahlJr , C. A., Guenther, P. R., Waterman, L. S., & Chin, J. F. (1976). Atmospheric carbon dioxide variations at Mauna lao observatory. *Tellus*, 28(6), 538–551.

Kulish, M., & Pagan, A. (2021). Turning point and oscillatory cycles: Concepts, measurement and use. *Journal of Economic Surveys*, 35(4), 977–1006.

Maddanu, F. (2022). A harmonically weighted filter for cyclical long memory processes. *AStA Advances in Statistical Analysis*, 106, 49–78.

McElroy, T., & Politis, D. N. (2024). Estimating the spectral density at frequencies near zero. *Journal of the American Statistical Association*, 119(545), 612–624.

Proietti, T., & F. Maddanu (2024). Modelling cycles in climate series: The fractional sinusoidal waveform process. *Journal of Econometrics* 239(1), 105299.

Sowell, F. (1992). Maximum likelihood estimation of stationary univariate fractionally integrated time series models. *Journal of Econometrics*, 53(1–3), 165–188.

Downloaded from https://www.cambridge.org/core. IP address: 92.41.158.104, on 12 Aug 2026 at 10:47:18, subject to the Cambridge Core terms of use, available at https://www.cambridge.org/core/terms. https://doi.org/10.1017/S0266466626100504